

Mermin-Ho vortex in ferromagnetic spinor Bose-Einstein condensates

T. Mizushima, K. Machida and T. Kita¹

Department of Physics, Okayama University, Okayama 700-8530, Japan,

¹*Division of Physics, Hokkaido University, Sapporo 060-0810, Japan*

(Dated: November 14, 2018)

The Mermin-Ho and Anderson-Toulouse coreless non-singular vortices are demonstrated to be thermodynamically stable in ferromagnetic spinor Bose-Einstein condensates with the hyperfine state $F = 1$. The phase diagram is established in a plane of the rotation drive vs the total magnetization by comparing the energies for other competing non-axis-symmetric or singular vortices. Their stability is also checked by evaluating collective modes.

PACS numbers: 03.75.Fi, 67.57.Fg, 05.30.Jp

Topological structure plays an important and decisive role in various research fields, ranging from condensed matter physics to high energy physics. They provide a common framework to connect diverse fields, enhancing mutual understanding[1].

Recent advance of experimental techniques on Bose-Einstein condensation (BEC) prompts us to closely and seriously look into theoretical possibilities which were mere imagination for theoreticians in this field. This is particularly true for spinor BEC where all hyperfine states of an atom Bose-condensed simultaneously, keeping these “spin” states degenerate and active. Recently, Barrett et al [3] have succeeded in cooling ^{87}Rb with the hyperfine state $F = 1$ by all optical methods without resorting to a usual magnetic trap in which the internal degrees of freedom is frozen. Since the spin interaction of the ^{87}Rb atomic system is ferromagnetic, based on the refined calculation of the atomic interaction parameters by Klausen et al[4], we now obtain concrete examples of the three component spinor BEC ($F = 1$, $m_F = 1, 0, -1$) for both antiferromagnetic (^{23}Na)[5] and ferromagnetic interaction cases. In the present spinor BEC the degenerate internal degrees of freedom play an essential role to determine the fundamental physical properties. There is a rich variety of topological defect structures, which are already predicted in the earlier studies[6, 7] on the spinor BEC. These are followed by others[8, 9, 10, 11, 12, 13, 14, 15, 16] who examine these topological structures more closely, such as skyrmion, monopole, meron or axis-symmetric or non axis-symmetric vortices both for antiferromagnetic and ferromagnetic cases.

Superfluid ^3He is analogous to the spinor BEC where the neutral Cooper pair possesses the orbital and spin degrees of freedom, thus the order parameter is a multi-component[17]. Among various topological structures, the Mermin-Ho (MH)[18] and Anderson-Toulouse (AT)[19] vortices of a coreless and non-singular l -vector texture are proposed in ^3He -A phase. These are an extremely interesting object to study if they exist. The MH vortex is expected to spontaneously appear in a cylindrical vessel without any external rotation as an equilib-

rium state because the rigid wall boundary imposes the l -vector perpendicular to the vessel wall. The MH vortex is stable also under slow rotation because of their non-singular coreless structures[20].

A similar topological structure, called skyrmion in general is proposed in the spinor BEC. Khawaja and Stoof[10] study a skyrmion in the ferromagnetic BEC with $F = 1$ and conclude that the skyrmion is not a thermodynamically stable object without rotation. Once created, its radius shrinks to vanish in spite of ingenious proposals[11, 12, 13, 14] as to how to create it and to detect it.

Here we demonstrate that in the ferromagnetic spinor BEC with $F = 1$ trapped in a harmonic potential the Mermin-Ho vortex and Anderson-Toulouse vortex are thermodynamically stable for a certain region of the external rotation frequency and the magnetization of the system. These vortices are stabler than the singular vortices and other possible non-axis symmetric vortices. This comes about because as a general tendency the ferromagnetic interaction leads to spatial phase separation of the three components ($\phi_1, \phi_0, \phi_{-1}$). Then by assigning different winding numbers $\langle 0, 1, 2 \rangle$ to these components in this order, they can be arranged so as to be effectively phase-separated in the radial direction, resulting in a concentric layered structure under a given magnetization. The central region is occupied by ϕ_1 , ϕ_0 is in the intermediate region, and ϕ_{-1} is in the outer layer. This ingenious non-singular coreless vortex acquires the angular momentum to effectively lower the total energy under rotation.

We start with the standard Hamiltonian by Ohmi and Machida[6], and Ho[7]: $H_{rot} = H - \int d\mathbf{r} \mathbf{\Omega} \cdot \sum_j \Psi_j^\dagger(\mathbf{r} \times \mathbf{p})\Psi_j$,

$$H = \int d\mathbf{r} \left[\sum_{ij} \Psi_i^\dagger \{h(\mathbf{r}) - \mu_i\} \Psi_j \delta_{ij} + \frac{g_n}{2} \sum_{ij} \Psi_i^\dagger \Psi_j^\dagger \Psi_j \Psi_i \right. \\ \left. + \frac{g_s}{2} \sum_{\alpha} \sum_{ijkl} \Psi_i^\dagger \Psi_j^\dagger (F_{\alpha})_{ik} (F_{\alpha})_{jl} \Psi_k \Psi_l \right]$$

where $h(\mathbf{r}) = -\frac{\hbar^2 \nabla^2}{2m} + V(\mathbf{r})$, $g_n = \frac{4\pi\hbar^2}{m} \cdot \frac{a_0+2a_2}{3}$, $g_s = \frac{4\pi\hbar^2}{m} \cdot \frac{a_2-a_0}{3}$. The subscripts are $\alpha = (x, y, z)$

and $i, j, k, l = (0, \pm 1)$ corresponding to the above three species. The chemical potentials for the three components; μ_i ($i = 0, \pm 1$) satisfy $\mu_1 + \mu_{-1} = 2\mu_0$. The scalar field $V(\mathbf{r}) = \frac{1}{2}m(2\pi\nu_r)^2(x^2 + y^2)$ is the external confinement potential such as an optical potential. The scattering lengths a_0 and a_2 characterize collisions between atoms with the total spin 0 and 2 respectively. As mentioned, the recent refined estimate[4] for ^{87}Rb concludes it ferromagnetic ($a_0 > a_2$) and $g_s/g_n = -0.01 \sim -0.005$. The external rotation frequency Ω is normalized by the harmonic confining frequency. It readily leads to the Gross-Pitaevskii (GP) equation extended to the three component order parameters: $[\{h(\mathbf{r}) - \mu_i + g_n \sum_k |\phi_k|^2\} \delta_{ij} + g_s \sum_\alpha \sum_{kl} \{(F_\alpha)_{ij} (F_\alpha)_{kl} \phi_k^* \phi_l\}] \phi_j = 0$. These coupled equations for the j -th condensate wave function $\phi_j = \langle \Psi_j \rangle$ ($j = 0, \pm 1$) are used to calculate various properties of a vortex in the following.

It is important to realize that in a real experimental situation the total number $N = \int d\mathbf{r} \sum_j |\phi_j|^2$ and the total magnetization $M = \int d\mathbf{r} \sum_j j |\phi_j|^2$ are fixed. In our case these quantities are fixed by adjusting the chemical potential (μ_0) and the fictitious magnetic field ($\mu' = \mu_1 - \mu_0$). The extended GP equation is solved numerically with two different methods for a two-dimensional disk: One is not to assume axis-symmetry. This calculation is backed up by the computation where the axis-symmetry is assumed. The actual calculations are done by discretizing two-dimensional space into 51×51 mesh. The vortex configuration is characterized by the combination of the winding number of each component. We denote it as $\langle w_1, w_0, w_{-1} \rangle$ where integers w_1, w_0, w_{-1} are the winding numbers of $\phi_1, \phi_0, \phi_{-1}$ respectively where w means the phase change by $2\pi w$ when the wave function goes around the phase singularity.

We have performed extensive search to find a stable vortex, starting with possible vortex configurations, covering a wide range of the ferromagnetic interaction strength $g_s/g_n = 0 \sim -0.02$ and examining various axis-symmetric and non-axis-symmetric vortices (see the classification of possible vortices in the axis-symmetric case[15, 16]). We use the following parameters: the mass of a ^{87}Rb atom $m = 1.44 \times 10^{-25} \text{ kg}$, the trapping frequency $\nu_r = 200 \text{ Hz}$, and the area density $n_z = 2.0 \times 10^3 / \mu\text{m}$. The results displayed here are $g_s/g_n = -0.02$.

The Mermin-Ho (MH) vortex is described by $(\phi_1, \phi_0, \phi_{-1}) = \sqrt{n(r)} (\cos^2 \frac{\beta}{2}, \sqrt{2} e^{i\phi} \sin \frac{\beta}{2} \cos \frac{\beta}{2}, e^{2i\phi} \sin^2 \frac{\beta}{2})$ where the bending angle $\beta(r)$ is $0 \leq \beta(r) \leq \pi$, ϕ is the polar angle in polar coordinates. The spin direction is denoted by the so-called l -vector[6] given by $\mathbf{l}(r) = \hat{z} \cos \beta + \sin \beta (\cos \phi \hat{x} + \sin \phi \hat{y})$ where β varies from $\beta(0) = 0$ to $\beta(R) = \frac{\pi}{2}$ for MH and to $\beta(R) = \pi$ for AT (R is the outer boundary of the cloud). Thus the spin moment is flared out to the radial direction and at the circumference it points outward for MH and

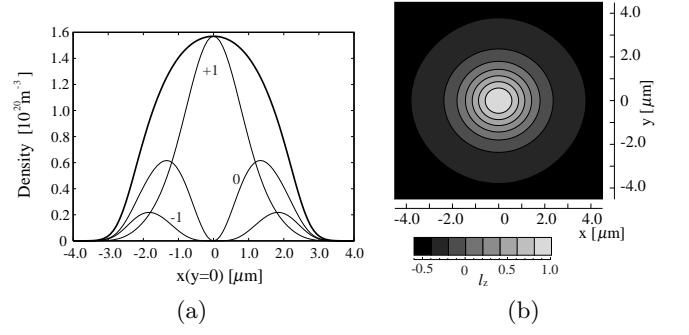


FIG. 1: Density profile of the condensates (a) and the density map of l_z -vector (b) for the $\langle 0, 1, 2 \rangle$ vortex at $\Omega = 0.35$ and $M/N=0.21$. The bold line is the total density $\sum_j |\phi_j|^2$ and the thin lines show the density of each component $|\phi_j|^2$.

downwards for AT (see for schematic l -vector structure Fig.18 in Ref.[17]). These vortices have the winding number combination $\langle 0, 1, 2 \rangle$ in our notation.

We show the calculated MH vortex in Fig.1 where the axis-symmetric density profiles for each component and the density map of l_z are displayed. It is seen that the central region of the harmonic trap is occupied by ϕ_1 with zero winding number $w_1 = 0$. The ϕ_0 component which has a singularity with $w_0 = 1$ at $r = 0$ is pushed outward while the ϕ_{-1} component occupies the circumference region because of $w_2 = 2$. Note that in the small r region the singular vortex with w behaves like $\propto r^w$. The resulting total density is coreless and non-singular. It has a smooth density variation described by a Gaussian form except for the outermost region.

In Fig.2 we show the spatial dependence of the l_z -component along the radial direction, namely, the spatial dependence of the bending angle $\beta(r)$ for the MH vortex. As the magnetization M decreases, the local magnetization changes from positive to negative values through zero. It means that the l -vector in the vortex flares out radially to orient almost horizontally $\beta(r=R) = \frac{\pi}{2}$ for $M/N \sim 0.5$ and to point down for $\beta(r=R) = \pi$ for $M/N \sim 0$. The former (latter) corresponds literally to the Mermin-Ho (Anderson-Toulouse) vortex. This is simply because as M decreases, the spin-down component ϕ_{-1} with $w = 2$ increases in the outer region. Thus we can control these MH and AT vortices by merely changing the total magnetization. We notice that in superfluid $^3\text{He-A}$ phase the stability of the MH and AT vortices is guaranteed by the boundary condition at the wall of a vessel where the l -vector is constraint to be parallel to the wall surface[17]. Here the situation is completely different; we impose no constraint on the l -vector direction. These vortex configurations are created naturally under the condition of a given total number and magnetization, both of which are well controlled in a harmonic trap experiment.

This difference in the two systems is rather remark-

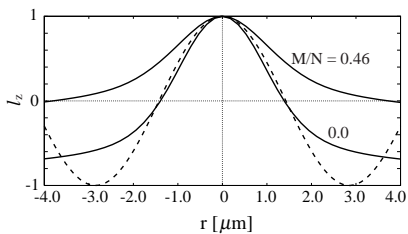


FIG. 2: Spatial dependence of the l_z -component along the radial direction at $M/N=0, 0.46$, and $\Omega = 0.37$. The dashed line shows $\cos\beta(r)$ with the bending angle $\beta(r) = \pi r/R$ ($R = 2.85\mu\text{m}$) for the AT vortex.

able and interesting. In our case MH or AT vortex comes about purely due to the spin interaction, which is written as $\propto |g_s||2\phi_1(r)\phi_{-1}(r) - \phi_0(r)|^2$. This term favors the mutual phase segregation[15, 16]. If $\phi_1(r) \neq 0$ and $\phi_{-1}(r) \neq 0$, $\phi_0(r)$ comes in, explaining the concentric layered structure. In fact, in the antiferromagnetic case the similar calculation shows that the MH and AT vortices are never stabilized under a similar condition[16, 21].

We have done extensive search for determining the region for the $\langle 0, 1, 2 \rangle$ vortex of the MH and AT in the plane of Ω vs M/N . We check our computation by starting with a certain initial vortex configuration, allowing non-axis-symmetric vortex. We end up with the axis-symmetric MH and AT vortices where these are stable. The stability for these vortices is also examined from the two aspects: one is the global stability and the other is local stability in the energy landscape. The global stability means comparing the relative energy of various vortices and vortex free state to select out the lowest energy state. The local stability is discussed shortly.

The resulting phase diagram is displayed in Fig.3 where a large area is occupied by the $\langle 0, 1, 2 \rangle$ vortex, including MH and AT. Near $M \sim 0$ the non-axis-symmetric $\langle 1, 1, 1 \rangle$ vortex and near $M/N \sim 1$, $\langle 1, 0, -1 \rangle$ vortex are stabilized. We find a large empty region in the intermediate M/N region where no vortex and vortex-free state are stabilized at all because the phase separation in the ferromagnetic case prevents forming a uniform mixture of the three components even when the circulation is absent for the vortex-free state. This is in contrast with the antiferromagnetic case in which everywhere is occupied by a stable phase.

It is noted that the focused frequency region $\Omega = 0.38$ corresponds to the single vortex region in the scalar BEC case[22] beyond which multiple vortex state must be seriously considered, thus the present single vortex consideration is justified in the lower frequencies.

We examine various competing vortices, including a singular vs non-singular and axis-symmetric vs non-axis-symmetric vortices. In particular, since for axis-symmetric vortices the winding number combination of the three components $\langle w_1, w_0, w_{-1} \rangle$ is restricted to $2w_0 =$

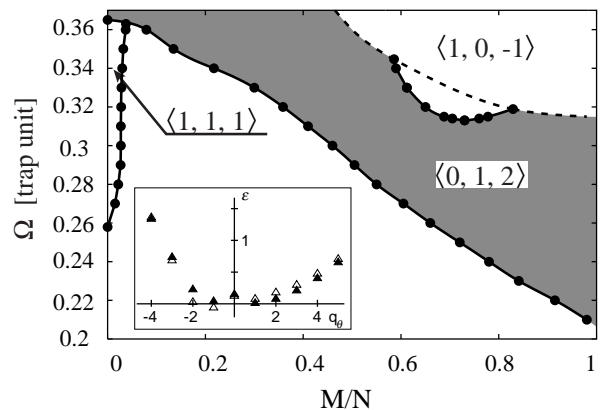


FIG. 3: Phase diagram in the ferromagnetic state. The lowest eigenvalues along q_θ at $\Omega=0.3$ are displayed in the inset. Triangles: $M/N=0.2$ and filled triangles: 0.75 .

$w_1 + w_{-1}$, we exhaust all the possible vortices with w_1, w_0, w_{-1} smaller than unity[16]. Note that MH and AT belong to this axis-symmetry category.

The $\langle 1, 1, 1 \rangle$ vortex shown in Fig. 4 is non-singular and non-axis-symmetric which is stable in low M/N . This $\langle 1, 1, 1 \rangle$ vortex is advantageous because (A) it does not contain the higher winding number. It generally leads to collapse fewer winding number vortex, such as $2 \rightarrow 1 + 1$ vortices. (B) The overall condensation energy is gained by placing their singularities off the trap center where the potential energy is minimum. (C) As Ω increases, the two separate singularities of ϕ_1 and ϕ_{-1} adjust their mutual distance from the center so as to maximize the angular momentum \vec{L} in order to save the energy $-\vec{\Omega} \cdot \vec{L}$. In this sense this configuration is flexible against varying Ω . These reasons explain why this vortex survives along the Ω -axis near $M/N \sim 0$ in Fig.3.

In contrast, the $\langle 0, 1, 2 \rangle$ vortex contains the higher winding number 2 for ϕ_{-1} , which makes it less advantageous against the $\langle 1, 1, 1 \rangle$ vortex. However, upon varying M , this vortex is quite flexible by adjusting the particle numbers for the three components; As M increases, the number of ϕ_1 grows smoothly relative to the rests. The non-winding ϕ_1 component works as a “pinning” center for the remaining ϕ_0 and ϕ_{-1} . In particular, ϕ_{-1} with $w_{-1} = 2$ is stabilized by the presence of ϕ_1 . Therefore as M increases or ϕ_1 grows, the MH and AT vortices become more and more stable. This explains that the critical frequency, or the lower phase boundary of MH in Fig.3 becomes less as M increases. As for the $\langle 1, 1, 1 \rangle$ vortex, in comparison, is not flexible enough for varying M because the symmetric arrangement of the two singularities in ϕ_1 and ϕ_{-1} around the center (see Fig.4) becomes unbalanced as ϕ_1 component grows while ϕ_{-1} shrinks. Thus it is confined in a narrow thin region near $M/N \sim 0$ (see Fig.3).

The $\langle 1, 0, -1 \rangle$ vortex, (not shown here, see Fig.3 in

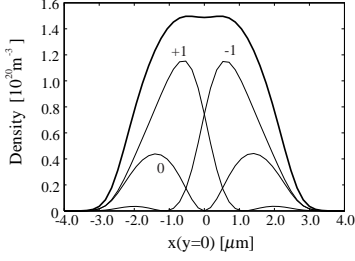


FIG. 4: Density profile of the condensates for the non-axis-symmetric $\langle 1, 1, 1 \rangle$ vortex in $\Omega = 0.35$ and $M/N=0.0$. The bold line is the total density $\sum_j |\phi_j|^2$ and the thin lines show the density of each component $|\phi_j|^2$.

Ref. [15]) is stabilized in larger M/N and higher Ω region because in this vortex the dominant component ϕ_1 has the winding number 1, which can effectively lower the rotation energy.

Having finished the “global” stability of the MH and AT vortices, we now turn to the “local” stability, that is, the stability against a small perturbation. This is done by solving the extended Bogoliubov equations to the three components under the axis-symmetric situation[15]: $\sum_j \{A_{ij}u_q(\mathbf{r}, j) - B_{ij}v_q(\mathbf{r}, j)\} = \varepsilon_q u_q(\mathbf{r}, i)$, and $\sum_j \{B_{ij}^*u_q(\mathbf{r}, j) - A_{ij}^*v_q(\mathbf{r}, j)\} = \varepsilon_q v_q(\mathbf{r}, i)$ where $A_{ij} = \hbar(\mathbf{r})\delta_{ij} - \mu_i\delta_{ij} + g_n \{\sum_k |\phi_k|^2 \delta_{ij} + \phi_i \phi_j^*\} + g_s \sum_\alpha \sum_{kl} [(F_\alpha)_{ij}(F_\alpha)_{kl} \phi_k^* \phi_l + (F_\alpha)_{il}(F_\alpha)_{kj} (\phi_k^* \phi_l)]$, $B_{ij} = g_n \phi_i \phi_j + g_s \sum_\alpha \sum_{kl} [(F_\alpha)_{ik} \phi_k (F_\alpha)_{jl} \phi_l]$, $u_q(\mathbf{r}, i)$ and $v_q(\mathbf{r}, i)$ are the q -th eigenfunctions with the spin i and ε_q corresponds to the q -th eigenvalue. Since this gives the excitation spectrum of the system, the negative energy relative to the condensation energy at zero implies the local intrinsic instability of the putative vortex in the energy landscape. We have performed the extensive computation to check this local stability for MH vortex and other axis-symmetric vortices against a small perturbation. As expected, the lower phase boundary of the MH in Fig.3 coincides almost completely with the local stability region, below which the lowest excitation mode with the angular momentum $q_\theta = -1$ for the positive external rotation ($\vec{\Omega} > 0$) becomes negative (see the inset in Fig.3). The upper boundary of the $\langle 0, 1, 2 \rangle$ vortex in Fig.3 indicates that the lowest excitation mode with mainly $q_\theta = +1$ becomes negative (see the inset in Fig.3). Thus the global stability mentioned roughly corresponds to the present local stability. Therefore, it is concluded that the MH and AT vortices are stable and robust in the ferromagnetic spinor BEC.

It is easy to calculate the total angular momentum L in MH vortex which is given by $L/\hbar = N_0 + 2N_{-1}$ (N_i is the particle number of the i -component). Since $M = N_1 - N_{-1}$ and $N = N_1 + N_0 + N_{-1}$, the total angular momentum per particle is found to be $\frac{L}{\hbar N} = 1 - \frac{M}{N}$. This simple formula means that at $M = 0$, ϕ_0 with $w_0 = 1$ carries all the angular momentum as in the usual scalar

vortex, and at $M = N$, $L = 0$ because ϕ_1 has no winding. At $\frac{M}{N} = \frac{1}{2}$, $\frac{L}{\hbar N}$ is half, implying that in the MH vortex the angular momentum per particle is exactly $\hbar/2$.

In summary, we have shown that the Mermin-Ho and Anderson-Toulouse vortices are thermodynamically stable under a certain rotation drive and the total magnetization of the system, both of which are experimentally well-controlled parameters. We have examined their stability by two methods, local and global ones in the energy landscape, coinciding with the earlier conclusion that these are unstable under no rotation drive[10]. These intriguing objects might be detected by various ways, such as optically by utilizing the Faraday rotation which images the spatial magnetic pattern of these vortices. A favorable experiment is to use an oblate ellipsoidal shaped system to mimic our disk calculation. An elongated cigar system may not be appropriate, which induces the phase separation along the long axis.

We thank T. Ohmi and T. Isoshima for valuable discussions.

-
- [1] R. Rajaraman, *Solitons and Instanton* (North-Holland, Amsterdam, 1982). N.D. Mermin, Rev. Mod. Phys. **51**, 591 (1979).
 - [2] A.J. Leggett, Rev. Mod. Phys. **73**, 307 (2001).
 - [3] M. Barrett, et al., Phys. Rev. Lett. **87** 010404 (2001).
 - [4] N.N. Klausen, et al., Phys. Rev. A **64**, 053602 (2001).
 - [5] J. Stenger, et al., Nature **369**, 345 (1998).
 - [6] T. Ohmi and K. Machida, J. Phys. Soc. Jpn. **67**, 1822 (1998).
 - [7] T.-L. Ho, Phys. Rev. Lett. **81**, 742 (1998).
 - [8] S.-K. Yip, Phys. Rev. Lett. **83**, 4677 (1999).
 - [9] U. Leonhardt and G. E. Volovik, JETP Lett. **72**, 46 (2000).
 - [10] U. Al Khawaja and H.T.C. Stoof, Nature **411**, 918 (2001), and Phys. Rev. A **64**, 043612 (2001).
 - [11] Karl-Peter Marzlin, et al., Phys. Rev. A **62**, 013602 (2000).
 - [12] Th. Busch and J.R. Anglin, Phys. Rev. A **60**, R2669 (1999).
 - [13] S. Tuchiya and S. Kurihara, J. Phys. Soc. Jpn. **70**, 1182 (2001).
 - [14] J.-P. Martikainen, et al, cond-mat/0106301.
 - [15] T. Isoshima, et al., J. Phys. Soc. Jpn. **70**, 1604 (2001).
 - [16] T. Isoshima and K. Machida, cond-mat/0201507.
 - [17] M.M. Salomaa and G.E. Volovik, Rev. Mod. Phys. **59**, 533 (1987).
 - [18] N.D. Mermin and Tin-Lun Ho, Phys. Rev. Lett. **36**, 594 (1976).
 - [19] P.W. Anderson and G. Toulouse, Phys. Rev. Lett. **38**, 508 (1977).
 - [20] See for recent advance on this subject, R. Blaauwgeers, et al., Nature **404**, 471 (2000).
 - [21] T. Mizushima et al., private communication.
 - [22] T. Isoshima and K. Machida, Phys. Rev. A **60**, 3313 (1999).